Journal of Construction and Engineering Technology
Journal homepage: www.journal.fstu.uz

NUMERICAL AND EXPERIMENTAL ANALYSIS OF PRESSURE LOSS IN CYLINDRICAL AIR DUCT

Giyosiddin Mamatisayev and Barkhayot Maksitaliev

Fergana State Technical University, Fergana, Uzbekistan
*Correspondence: maxsitaliyevbarxayot@gmail.com

Abstract

This study investigates the pressure loss in ventilation ducts by experimental measurements and numerical simulations in order to improve the accuracy of calculations in the design of ventilation systems. The experiments were conducted in a cylindrical duct with a diameter of 100 mm and a length of 1.5 m on the PAXP-VV-K "Ventilation System Testing" laboratory stand. The air velocity was varied in the range of 2.3–3.8 m/s (Re = 1.5×10^4–2.5×10^4), and the pressure drop was measured using differential manometers and pressure sensors, achieving high repeatability (standard deviation < 3 %; U(ΔP) = 11–19 %, k = 2). Numerical modeling was performed in the COMSOL Multiphysics program using the Realizable k-ε turbulence model. The measured loss was 4.5–8.5 Pa, whereas friction theory gives 1.4–3.3 Pa and the CFD simulation 2.6–3.8 Pa, i.e. the CFD values are 50–58 % lower than the measured ones. The discrepancy exceeds the standard measurement uncertainty by a factor of 7–10, so the model does not satisfy the ASME V&V 20 validation criterion; the excess loss ($K_{tot} - \lambda l/d \approx 0.5$–$0.65$) is of the magnitude of local losses in the measured path.

Keywords: Pressure drop, turbulent flow, CFD modeling, ventilation ducts, friction coefficient, Reynolds number, k-ε turbulence model, uncertainty analysis, validation, PAXP-VV-K stand.

1. Introduction

The energy efficiency and indoor climate of modern buildings are one of the main factors determining their usability and environmental sustainability. About half of the energy used in buildings is spent on heating, ventilation and air conditioning (HVAC) systems [1]. In this regard, the need to minimize aerodynamic losses in the design of ventilation systems is becoming increasingly urgent. The quality of indoor air and heat balance of buildings are directly dependent on efficient ventilation systems, and their energy consumption is determined by the aerodynamic resistance in the duct networks. Pressure loss in ventilation ducts directly affects the electric energy consumption of fans and determines the overall energy efficiency of the system.

Currently, in Uzbekistan, the demand for HVAC systems in newly constructed modern public and residential buildings is increasing sharply. Climate change and urbanization processes are raising the requirements for indoor environmental quality to a higher level [2, 3]. The pressure loss (ΔP) occurring during air flow in ventilation ducts is a decisive factor in the overall energy consumption of the system and the selection of fan parameters. Accurately calculated pressure loss allows minimizing energy consumption, reducing noise, and increasing system reliability. The Darcy-Weisbach equation, Moody diagram, and Colebrook-White correlation [4–6], which are the main tools of classical hydraulics for accurately predicting pressure loss, have been used in engineering practice for many years. Although these methods provide reliable results for smooth and homogeneous ducts (accuracy about ±5 % [5]), their accuracy is limited in complex geometries (bends, diffusers, branches), changes in wall smoothness, and high turbulence conditions [7]. COMSOL Multiphysics [8] allows modeling of complex physical processes. Turbulence models include the k-ε model proposed by Launder and Spalding [9], the SST k-ω model improved by Menter [10], and the models developed by Spalart and Allmaras [11] and Durbin [12].

In recent decades, the development of numerical modeling CFD (Computational Fluid Dynamics) tools has created new opportunities in the design of ventilation systems. CFD methods, in particular,

Received: 11 February 2026
Revised: 05 October 2026
Accepted: 10 November 2026
https://doi.org/10.67846/jcet.2026.4297

approaches based on the Reynolds-averaged Navier-Stokes (RANS) equations, allow for detailed visualization and quantitative assessment of the flow structure, velocity and pressure distribution in channels [8]. In modeling turbulent flows, two-equation models of the k-ε and k-ω families are the most common, and their various modifications (for example, Realizable k-ε and SST k-ω) provide optimal accuracy for various flow conditions [10, 13, 14]. The reliable use of numerical models in engineering practice is limited by the need to validate them with experimental data and with a quantified numerical uncertainty [15–18]. The validation process is an indispensable condition for checking how accurately the CFD model reflects the real physical process, adjusting the model parameters, and determining the limits of its applicability. Only numerical models validated by experimental measurements become a reliable tool in the design and optimization of ventilation systems.

The main objective of this study is to determine the pressure loss in a straight ventilation duct by experimental measurements and numerical simulation and to assess the accuracy of the CFD model (Realizable k-ε) by comparing it with the measurements and with classical friction theory. The PAXP-VV-K "Ventilation System Testing" laboratory stand, which was designed in accordance with international standards and has high-precision measuring instruments, was used in the study.

Many studies have been devoted to the calculation of pressure loss in ventilation ducts. Moody [5] proposed a diagram of the friction factor for pipes in his classic work, and Colebrook [6] derived an empirical formula for the transition region between smooth and rough pipes.

However, many studies do not sufficiently cover experimental validation in practical ventilation systems. This study aims to fill this gap, combining experimental and numerical methods.

2. Materials and Methods

The research aimed to determine the pressure loss in a straight smooth plastic duct (d = 100 mm, l = 1.5 m, l/d = 15) and to compare it with theory and CFD. The experiments were conducted on the PAXP-VV-K "Ventilation system testing" laboratory stand (Figure 1). This stand is equipped with the main elements of ventilation systems: air ducts, a ventilator, measuring instruments and sensors that control air speed and humidity. The stand makes it possible to model the operating mode of a ventilation system, to determine air-exchange parameters and to evaluate microclimate indicators.

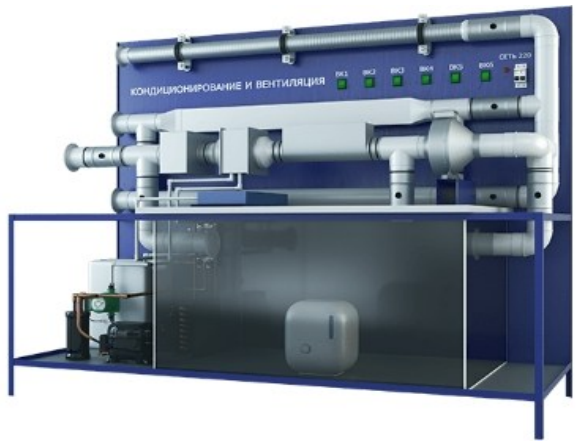


Figure 1. PAXP-VV-K "Ventilation system testing" laboratory stand.

Experimental method. Experimental measurements were carried out on the PAXP-VV-K "Ventilation system testing" laboratory stand. The stand consists of the following (Table 1) main components:

Table 1

Parameter	Instrument	Range	Accuracy
Pressure loss (Δp)	Differential manometer (TSI 8705)	0-2000 Pa	±0.5 Pa or ±1 %
Local pressure (p)	Piezoresistive sensors (Honeywell 40PC)	0-5000 Pa	±0.25%
Flow rate (Q)	Pitot-static tubes + anemometer	–	±2%
Air velocity (V)	Hot-wire anemometer (Testo 425)	0-20 m/s	±0.03 m/s
Temperature (T)	Thermocouple (K-type)	0-50°C	±0.5°C
Relative humidity (RH)	Capacitive sensor	0-100%	±2%
Atmospheric pressure (P_{atm})	Barometer	90-110 kPa	±0.1 kPa

The experiment comprised six measurement points (Table 2). At each point the fan speed was changed, which changed the air flow rate and the pressure difference. To determine the flow regime in the duct, the Reynolds number was calculated from the air velocity and the pipe diameter (Eq. (1)). Each point was repeated several times; V is the bulk (mean) air velocity. The air properties were taken at 20 °C and 101.325 kPa: ϱ = 1.204 kg/m³ and ν = 1.516×10⁻⁵ m²/s. The Reynolds numbers ranged from 15 174 to 25 070 (u(Re)/Re = 0.6–0.8 %). The hydrodynamic entrance length, $l_h/d \approx 1.359Re^{1/4}–4.4Re^{1/6}$ = 15–24 [19], is not shorter than the duct length (l/d = 15); therefore, the flow in the test section is still developing.

$$\mathrm{Re} = \frac{Vd}{\nu} \tag{1}$$

The hydraulic friction coefficient was calculated with the Altshul formula [20], which, unlike the Shifrinson formula $\lambda = 0.11(K_e/d)^{0.25}$ valid only for fully rough flow, takes the Reynolds number into account:

$$\lambda = 0.11\left(\frac{K_e}{d} + \frac{68}{\mathrm{Re}}\right)^{0.25} \tag{2}$$

where K_e is the equivalent roughness height, taken as 0.01 mm ($K_e/d = 10^{-4}$) for smooth plastic pipes [21]. The pressure drop due to friction along the duct length was determined from the Darcy–Weisbach formula [22]:

$$\Delta P = \lambda \frac{l}{d}\frac{\rho V^2}{2} \tag{3}$$

where l is the duct length, ϱ is the air density and V is the bulk velocity.

The measured pressure drop is expressed by the total loss coefficient:

$$K_{\mathrm{tot}} = \frac{2\Delta P}{\rho V^2} = \lambda \frac{l}{d} + \sum K_{\mathrm{loc}} \tag{4}$$

where ΣK_{loc} is the sum of the local loss coefficients. The relative deviation η of a theoretical or CFD value X from the measured value is defined as

$$\eta = \frac{X - \Delta P_{\mathrm{exp}}}{\Delta P_{\mathrm{exp}}} \tag{5}$$

where ΔP_{exp} is the measured pressure loss.

Table 2. Pressure loss: measured (ΔP_{exp}) with expanded uncertainty U(ΔP), theoretical (ΔP_{theor}, Eqs. (2), (3)) and CFD (ΔP_{CFD}) values, and their relative deviations η (Eq. (5)).

№	V (m/s)	Re	$\Delta P_{exp} \pm U(\Delta P)$ (Pa)	ΔP_{theor} (Pa)	ΔP_{CFD} (Pa)	η_{theor} (%)	η_{CFD} (%)
1	2.3	15 174	4.5 ± 0.86 †	1.37	n/a	−70	n/a
2	3.05	20 122	5.5 ± 0.88	2.24	2.55	−59	−54
3	3.3	21 771	6.5 ± 0.90	2.58	2.93	−60	−55
4	3.6	23 750	7.5 ± 0.93	3.00	3.41	−60	−55
5	3.7	24 410	8.5 ± 0.96	3.15	3.59	−63	−58
6	3.8	25 070	7.5 ± 0.93 ‡	3.30	3.77	−56	−50

Uncertainty analysis

The measurement uncertainty was evaluated following the GUM [23]. The combined standard uncertainty u(ΔP) includes the manometer accuracy (±0.5 Pa, rectangular distribution), the reading resolution (1 Pa, rectangular distribution) and the repeatability (3 % of the reading):

$$u(\Delta P) = \sqrt{u_m^2 + u_{\mathrm{res}}^2 + u_{\mathrm{rep}}^2} \tag{6}$$

where $u_m = u_{res} = 0.5/\sqrt{3} \approx 0.29$ Pa and $u_{rep} = 0.03\Delta P$. The expanded uncertainty is

$$U(\Delta P) = k \cdot u(\Delta P) \tag{7}$$

with the coverage factor k = 2. For the studied points u(ΔP) = 0.43–0.48 Pa and U(ΔP) = 0.86–0.96 Pa, i.e. 11–19 % of the reading (Table 2).

Data consistency

† Case 1: $K_{tot} = 1.41$, which is 43 % above the mean of cases 2–5 (0.99); this point has the largest relative uncertainty (U(ΔP)/ΔP = 19 %). ‡ Case 6 is non-monotonic: ΔP = 7.5 Pa at 3.8 m/s is lower than ΔP = 8.5 Pa at 3.7 m/s, whereas $K_{tot} = 0.99$ would give 8.6 Pa; this point is flagged in Fig. 2 and should be confirmed by a repeated measurement.

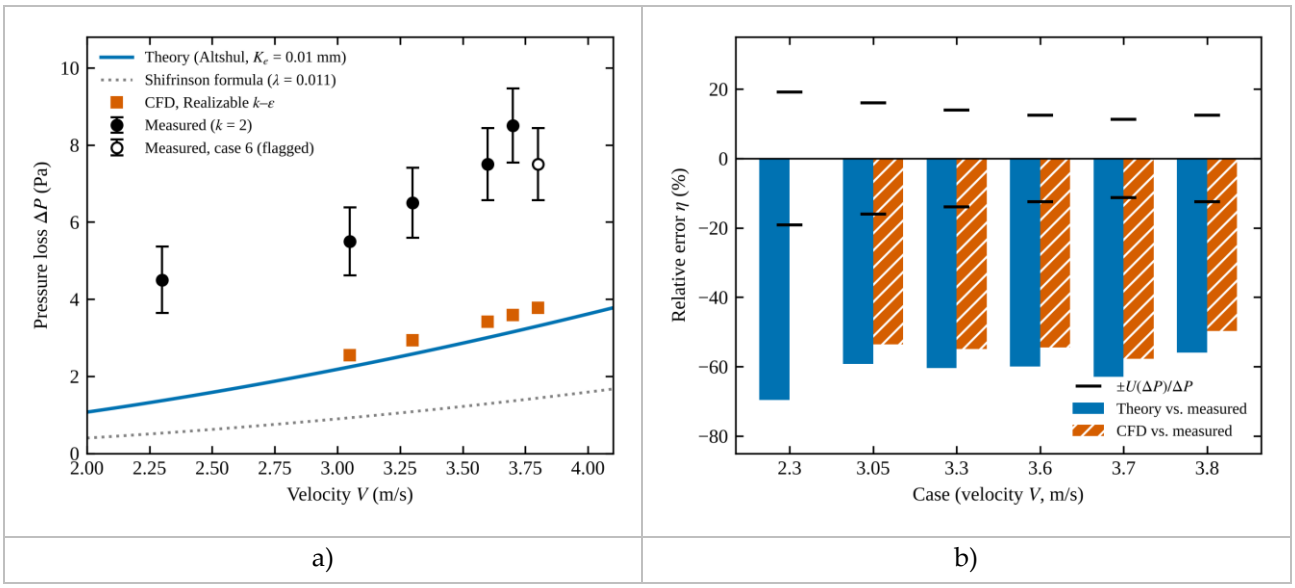


Figure 2. Pressure loss in the duct: a) measured values (error bars: k = 2), theory and CFD; b) relative deviations η by case (V, m/s).

3. Mathematical analysis

Law of conservation of mass (Continuity equation):

$$\frac{\partial(\rho u)}{\partial x}+\frac{\partial(\rho v)}{\partial y}+\frac{\partial(\rho w)}{\partial z}=0 \qquad (8)$$

For an incompressible fluid:

$$\frac{\partial u}{\partial x}+\frac{\partial v}{\partial y}+\frac{\partial w}{\partial z}=0 \qquad (9)$$

Reynolds-averaged Navier–Stokes equations (momentum conservation)

X-direction:

$$\rho\left(u\frac{\partial u}{\partial x}+v\frac{\partial u}{\partial y}+w\frac{\partial u}{\partial z}\right)=-\frac{\partial p}{\partial x}+\frac{\partial}{\partial x}\left[2\mu\frac{\partial u}{\partial x}\right]+\frac{\partial}{\partial y}\left[\mu\left(\frac{\partial u}{\partial y}+\frac{\partial v}{\partial x}\right)\right]+\frac{\partial}{\partial z}\left[\mu\left(\frac{\partial u}{\partial z}+\frac{\partial w}{\partial x}\right)\right]$$
$$+\frac{\partial}{\partial x}\left(-\rho\overline{u'u'}\right)+\frac{\partial}{\partial y}\left(-\rho\overline{u'v'}\right)+\frac{\partial}{\partial z}\left(-\rho\overline{u'w'}\right)+F_x \qquad (10)$$

Y-direction:

$$\rho\left(u\frac{\partial v}{\partial x}+v\frac{\partial v}{\partial y}+w\frac{\partial v}{\partial z}\right)=-\frac{\partial p}{\partial y}+\frac{\partial}{\partial x}\left[\mu\left(\frac{\partial v}{\partial x}+\frac{\partial u}{\partial y}\right)\right]+\frac{\partial}{\partial y}\left[2\mu\frac{\partial v}{\partial y}\right]+\frac{\partial}{\partial z}\left[\mu\left(\frac{\partial v}{\partial z}+\frac{\partial w}{\partial y}\right)\right]$$
$$+\frac{\partial}{\partial x}\left(-\rho\overline{u'v'}\right)+\frac{\partial}{\partial y}\left(-\rho\overline{v'v'}\right)+\frac{\partial}{\partial z}\left(-\rho\overline{v'w'}\right)+F_y \qquad (11)$$

Z-direction:

$$\rho\left(u\frac{\partial w}{\partial x}+v\frac{\partial w}{\partial y}+w\frac{\partial w}{\partial z}\right)=-\frac{\partial p}{\partial z}+\frac{\partial}{\partial x}\left[\mu\left(\frac{\partial w}{\partial x}+\frac{\partial u}{\partial z}\right)\right]+\frac{\partial}{\partial y}\left[\mu\left(\frac{\partial w}{\partial y}+\frac{\partial v}{\partial z}\right)\right]+\frac{\partial}{\partial z}\left[2\mu\frac{\partial w}{\partial z}\right]$$
$$+\frac{\partial}{\partial x}\left(-\rho\overline{u'w'}\right)+\frac{\partial}{\partial y}\left(-\rho\overline{v'w'}\right)+\frac{\partial}{\partial z}\left(-\rho\overline{w'w'}\right)+F_z \qquad (12)$$

where $\rho\left(u\frac{\partial u}{\partial x}+v\frac{\partial u}{\partial y}+w\frac{\partial u}{\partial z}\right)$ are the convective acceleration terms, i.e. the acceleration resulting from the motion of air particles with their own velocity;

$u\frac{\partial u}{\partial x}$ is the axial convection;

$v\frac{\partial u}{\partial y}$ and $w\frac{\partial u}{\partial z}$ are the transverse convection terms;

$-\frac{\partial p}{\partial x}$ is the pressure-gradient term, the force created by the pressure difference;

a pressure drop in the flow direction ($\frac{\partial p}{\partial x}<0$) makes this term positive, i.e. it is the driving force of the flow;

$\frac{\partial}{\partial x}\left[2\mu\frac{\partial u}{\partial x}\right]+\frac{\partial}{\partial y}\left[\mu\left(\frac{\partial u}{\partial y}+\frac{\partial v}{\partial x}\right)\right]+\frac{\partial}{\partial z}\left[\mu\left(\frac{\partial u}{\partial z}+\frac{\partial w}{\partial x}\right)\right]$ are the viscous stresses arising from internal friction;

$\frac{\partial}{\partial x}\left(-\rho\overline{u'u'}\right)+\frac{\partial}{\partial y}\left(-\rho\overline{u'v'}\right)+\frac{\partial}{\partial z}\left(-\rho\overline{u'w'}\right)$ are the Reynolds stresses;

$-\rho\overline{u'v'} = \mu_t\left(\frac{\partial u}{\partial y}+\frac{\partial v}{\partial x}\right)$ is the additional stress caused by turbulent fluctuations (Boussinesq approximation, μ_t is the turbulent viscosity); these terms are the main source of resistance in turbulent flow;

F_x, F_y, F_z are the body (volume) forces.

Turbulent kinetic energy (k) equation

$$\rho\left(u\frac{\partial k}{\partial x}+v\frac{\partial k}{\partial y}+w\frac{\partial k}{\partial z}\right)=\frac{\partial}{\partial x}\left[\left(\mu+\frac{\mu_t}{\sigma_k}\right)\frac{\partial k}{\partial x}\right]+\frac{\partial}{\partial y}\left[\left(\mu+\frac{\mu_t}{\sigma_k}\right)\frac{\partial k}{\partial y}\right]+\frac{\partial}{\partial z}\left[\left(\mu+\frac{\mu_t}{\sigma_k}\right)\frac{\partial k}{\partial z}\right]+P_k-\rho\varepsilon \quad (13)$$

$k=\frac{1}{2}\left(u'^2+v'^2+w'^2\right)$ is the turbulent kinetic energy;

P_k is the production term (generation of turbulence by the velocity gradient);

ε is the dissipation rate (conversion of turbulent energy into heat);

$\sigma_k \approx 1.0$ is the turbulent Prandtl number for k;

$\mu_t=\rho C_\mu\frac{k^2}{\varepsilon}$ is the turbulent viscosity, where C_μ is a model constant (variable in the Realizable model [14]).

The production rate P_k is

$$P_k=\mu_t\left[2\left(\frac{\partial u}{\partial x}\right)^2+2\left(\frac{\partial v}{\partial y}\right)^2+2\left(\frac{\partial w}{\partial z}\right)^2+\left(\frac{\partial u}{\partial y}+\frac{\partial v}{\partial x}\right)^2+\left(\frac{\partial u}{\partial z}+\frac{\partial w}{\partial x}\right)^2+\left(\frac{\partial v}{\partial z}+\frac{\partial w}{\partial y}\right)^2\right] \quad (14)$$

Dissipation (ε) equation

$$\rho\left(u\frac{\partial \varepsilon}{\partial x}+v\frac{\partial \varepsilon}{\partial y}+w\frac{\partial \varepsilon}{\partial z}\right)=\frac{\partial}{\partial x}\left[\left(\mu+\frac{\mu_t}{\sigma_\varepsilon}\right)\frac{\partial \varepsilon}{\partial x}\right]+\frac{\partial}{\partial y}\left[\left(\mu+\frac{\mu_t}{\sigma_\varepsilon}\right)\frac{\partial \varepsilon}{\partial y}\right]+\frac{\partial}{\partial z}\left[\left(\mu+\frac{\mu_t}{\sigma_\varepsilon}\right)\frac{\partial \varepsilon}{\partial z}\right]+C_1\rho S\varepsilon-C_2\rho\frac{\varepsilon^2}{k+\sqrt{\nu\varepsilon}} \quad (15)$$

$S=\sqrt{2S_{ij}S_{ij}}$, $S_{ij}=\frac{1}{2}\left(\frac{\partial u_i}{\partial x_j}+\frac{\partial u_j}{\partial x_i}\right)$, is the scalar measure of the velocity gradient (modulus of the mean strain-rate tensor);

$C_1 \approx 1.44$, $C_2 \approx 1.92$ and $\sigma_\varepsilon \approx 1.3$ are the standard k-ε model constants [9]; the Realizable model [14] used here has $C_1=\max\left[0.43,\frac{\chi}{\chi+5}\right]$, $\chi=Sk/\varepsilon$, $C_2=1.9$, $\sigma_\varepsilon=1.2$ and a variable C_μ;

$\nu=\frac{\mu}{\rho}$ is the kinematic viscosity.

Equations (8)–(15) form the system of Reynolds-averaged equations that is closed by the Realizable k-ε model and solved numerically in COMSOL Multiphysics [8].

Numerical set-up

Steady incompressible isothermal RANS equations were solved in COMSOL Multiphysics [8] for a straight cylinder (d = 100 mm, l = 1.5 m). Inlet: uniform V = 2.3–3.8 m/s, turbulence intensity I = $0.16\mathrm{Re}^{-1/8}$ ≈ 4.5–4.8 %, turbulence length scale 0.07d; outlet: p = 0 (gauge); wall: smooth, no-slip; ϱ = 1.204 kg/m³, μ = 1.825×10^{-5} Pa·s. The Realizable k-ε model uses wall functions (δ_{w^+} = 11.06 [8]); the SST k-ω model requires $y^+ \approx 1$ (first cell 0.07–0.11 mm). The CFD pressure loss ΔP is the area-averaged static pressure at the inlet relative to the outlet (p = 0).

4. Mesh independence and validation

The discretisation error is quantified by the grid convergence index (GCI) [17], evaluated on three systematically refined meshes with a refinement ratio r ≥ 1.3:

$$\mathrm{GCI}=\frac{1.25\left|\frac{\varphi_1-\varphi_2}{\varphi_1}\right|}{r^p-1} \quad (16)$$

where φ = ΔP, the subscripts 1 and 2 denote the fine and the medium mesh, and p is the observed order of convergence. Following ASME V&V 20 [18], the comparison error is

$$E=S-D \quad (17)$$

where S is the simulated and D is the measured value. The model is considered validated if

$$|E| \le u_{\mathrm{val}}=\sqrt{u_{\mathrm{num}}^2+u_{\mathrm{input}}^2+u_D^2} \quad (18)$$

where u_{num} = GCI/2 is the numerical uncertainty, u_D = u(ΔP) is the experimental uncertainty and $u_{input} \approx 1$ % is the uncertainty of the input parameters.

For the five cases with CFD results (cases 2–6), |E| = 2.95–4.91 Pa (Table 2), which is 6.7–10.2 times u_D = 0.44–0.48 Pa. Criterion (18) could be satisfied only if $u_{num} \ge$ 2.9–4.9 Pa, i.e. a numerical uncertainty of the order of the simulated ΔP itself (98–136 %), which is not realistic for a mesh-converged solution. Therefore, the Realizable k-ε model is not validated by the present measurements, irrespective of the GCI value.

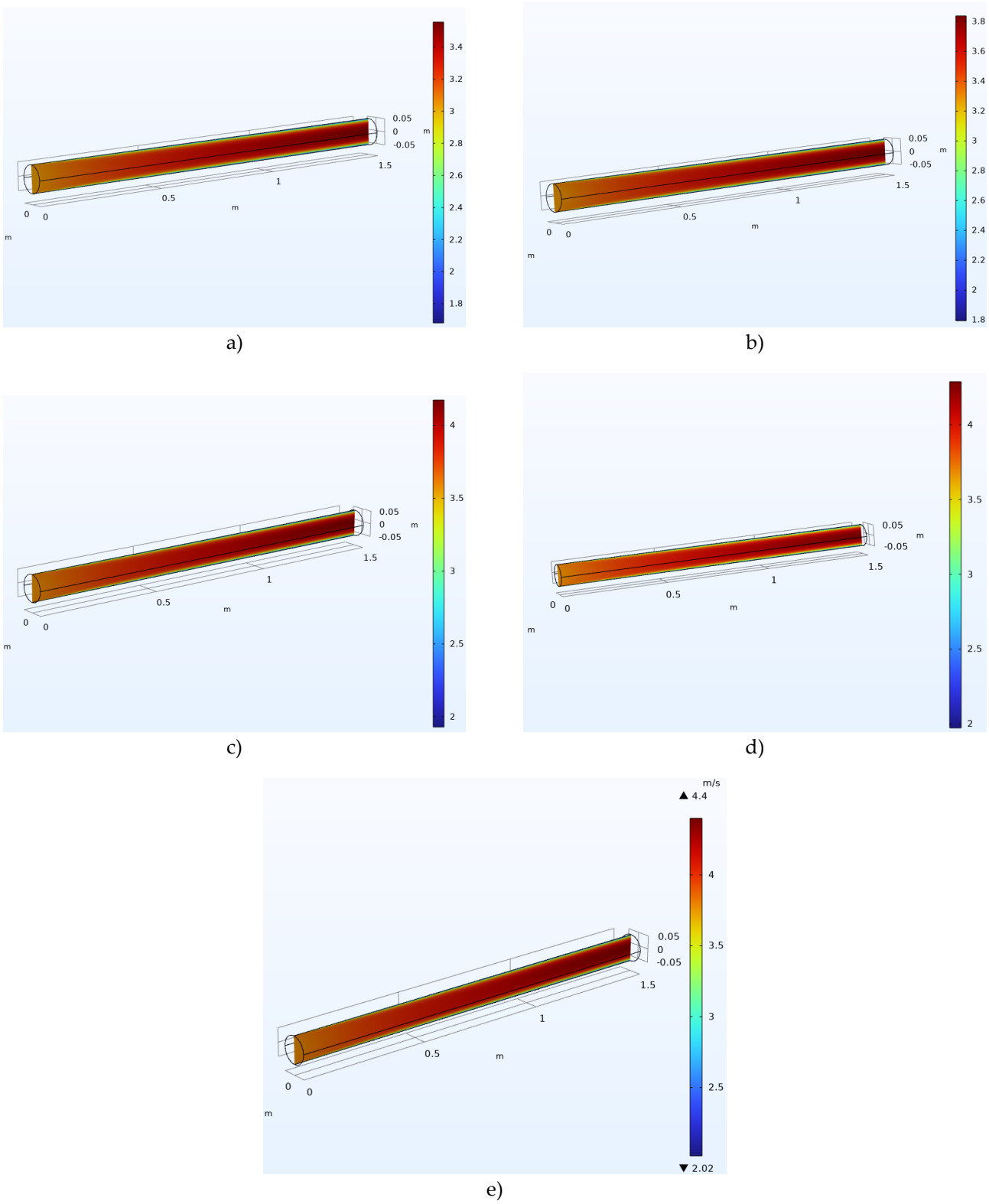


Figure 3. Velocity distribution (m/s) in the duct, CFD results for the inlet velocities a) 3.05; b) 3.3; c) 3.6; d) 3.7; e) 3.8 m/s (cases 2–6 of Table 2).

The following main features are observed in the velocity fields (Fig. 3a–e). In all velocity regimes (3.05–3.8 m/s) the velocity distribution is axially symmetric, with the maximum velocity at the centre of the channel; the radial profile deviates from the parabolic shape. Near the wall the velocity decreases sharply; the boundary layer thickness is about 2–3 mm and is the smallest (≈1.5 mm) at 3.8 m/s. At the inlet the velocity profile is flatter; at a distance of 1.5 m along the flow it approaches the developed shape ($U_{max}/V \approx 1.15$ against

≈ 1.21 for fully developed flow), and at Re > 20 000 the profile is flattened in the central zone. As the velocity increases, the velocity gradient increases and the maximum velocity is about 15 % higher than the mean velocity; the gradient near the wall reaches its maximum at the highest velocity. The non-zero wall velocity (≈ 1.8–2.3 m/s) results from the wall-function formulation.

5. Pressure difference

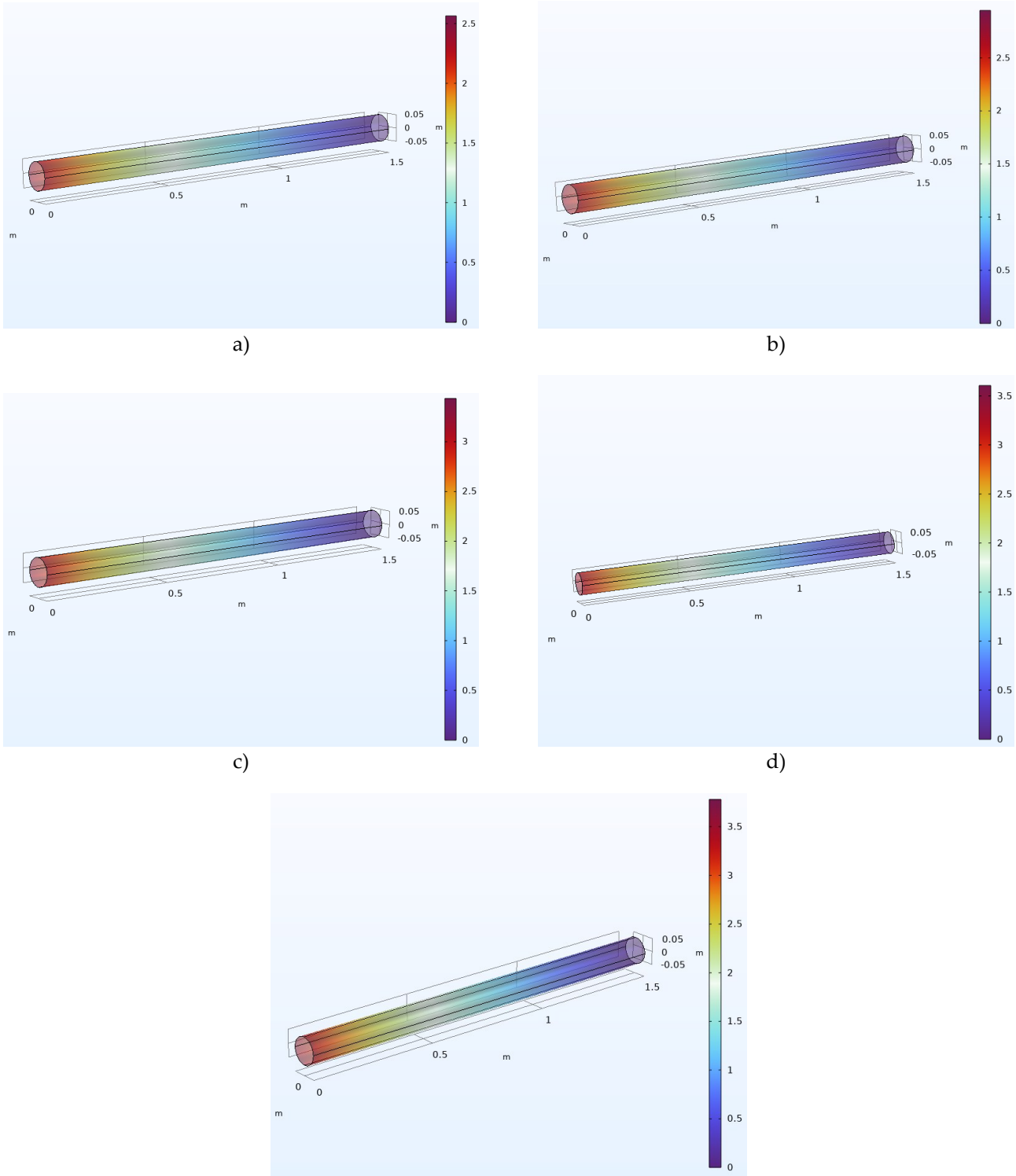


Figure 4. Static pressure distribution (Pa) along the duct, CFD results for the inlet velocities a) 3.05; b) 3.3; c) 3.6; d) 3.7; e) 3.8 m/s.

The following patterns are observed in the pressure distributions (Fig. 4a–e). The pressure drop along the duct length is almost linear (slightly steeper near the inlet, where the profile develops). The pressure over the cross-section is almost uniform, independent of the radius (difference of less than 0.5 %), which is typical for incompressible flow in a constant cross-section. The CFD pressure loss (inlet value of the colour scale, ±0.05 Pa) is 2.55–3.77 Pa for 3.05–3.8 m/s.

6. Velocity diagram

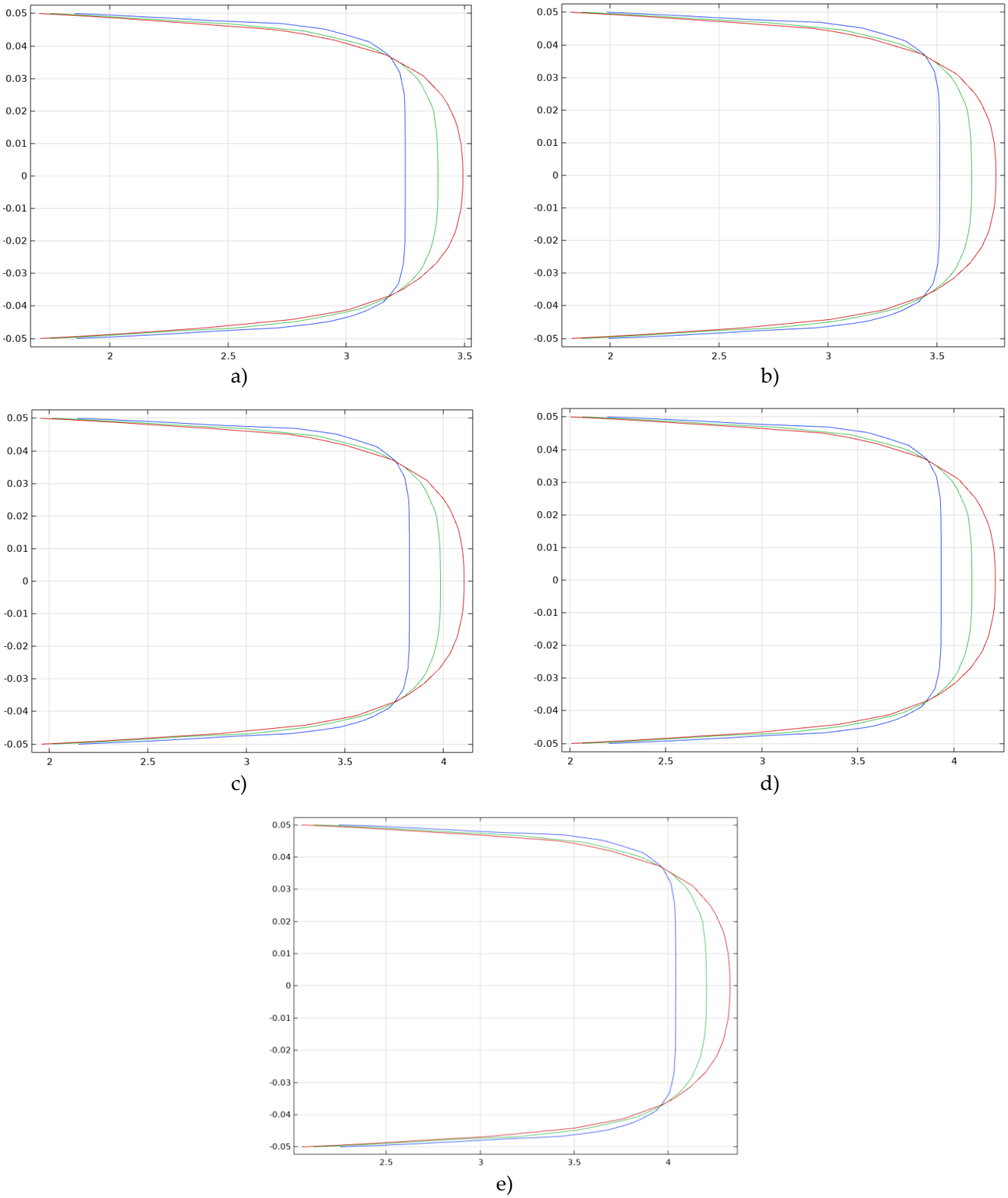


Figure 5. Velocity profiles (m/s) in the cross-section of the cylindrical channel (radial coordinate in m) for the inlet velocities a) 3.05; b) 3.3; c) 3.6; d) 3.7; e) 3.8 m/s.

As the air velocity increases (up to 3.8 m/s), the Reynolds number increases and the relative thickness of the near-wall region decreases (Fig. 5a–e). In turbulent flow the central zone is flatter and the boundary layer is steeper; at 3.8 m/s the profile has the most "filled" shape. This is favourable for reducing the energy losses in ventilation ducts, since the relative size of the steep-gradient zone near the wall decreases (λ falls from 0.029 to 0.025, Eq. (2)).

Comparison of experiment, theory and CFD

CFD (2.6–3.8 Pa) agrees with the Altshul theory (1.4–3.3 Pa) within about 14 % (developing flow in a duct of l/d = 15), but the measured loss is 2.0–2.4 times the CFD value (η = −50 to −58 %, Table 2, Fig. 2); $|E|$ exceeds u(ΔP) by a factor of 6.7–10.2, so criterion (18) is not satisfied. The measured K_{tot} = 0.86–1.03 exceeds the friction value λl/d = 0.38–0.40 by 0.5–0.65. Roughness cannot explain this (the Colebrook–White equation would require K_e ≈ 3–4 mm, whereas galvanised steel raises λ by ≤ 7 %); the excess is of the magnitude of a local loss (e.g. a sharp-edged entrance, K ≈ 0.5). To separate friction from local losses, the measurements should be repeated in a longer test section with the pressure taps located at least 25d downstream of the inlet and with ΔP ≳ 25 Pa (U(ΔP) ≈ 7 %).

7. Conclusions

The pressure loss in a straight smooth plastic duct (d = 100 mm, l = 1.5 m) was studied experimentally on the PAXP-VV-K laboratory stand and numerically in COMSOL Multiphysics (Realizable k-ε model) at V = 2.3–3.8 m/s (Re = 15 174–25 070). The following conclusions were obtained.

1) The measured pressure loss was 4.5–8.5 Pa with a repeatability (standard deviation) below 3 % and an expanded uncertainty U(ΔP) = 0.86–0.96 Pa (11–19 %, k = 2); the total loss coefficient was K_{tot} = 0.86–1.03 (cases 2–6). Two points deviate from the general trend (case 1: K_{tot} = 1.41; case 6: non-monotonic ΔP) and are flagged in Table 2 and Fig. 2.

2) The friction theory (Eqs. (2), (3); ΔP = 1.4–3.3 Pa) and the Realizable k-ε simulation (ΔP = 2.6–3.8 Pa) agree within about 14 %; thus the CFD model reproduces the friction loss of the developing flow in the duct (l/d = 15 is shorter than the entrance length of 15–24d).

3) The measured loss is 2.0–2.4 times the CFD value (η = −50 to −58 %) and 2.3–2.7 times the theoretical friction loss. The discrepancy exceeds the standard measurement uncertainty by a factor of 6.7–10.2, and the ASME V&V 20 criterion (Eq. (18)) is not satisfied in any case; the model is therefore not validated by the present measurements, irrespective of the grid-convergence result. A comparison of other turbulence models (SST k-ω, Spalart–Allmaras, Durbin) was not made in this study.

4) The excess of the measured total loss over the friction loss, $K_{tot} - \lambda l/d \approx 0.5–0.65$, cannot be explained by wall roughness (K_e ≈ 3–4 mm would be required, whereas galvanised steel raises λ by ≤ 7 %); it is of the magnitude of local losses in the measured path (e.g. a sharp-edged entrance, K ≈ 0.5), which are not included in the straight-duct model.

5) With increasing velocity the velocity profile becomes fuller ($U_{max}/V \approx 1.15$ at the outlet against ≈ 1.21 for fully developed flow), consistent with the decrease of λ from 0.029 to 0.025. The pressure decreases almost linearly along the duct and is uniform over the cross-section (deviation < 0.5 %), as is characteristic of incompressible flow in a constant cross-section.

6) For short ducts (l/d ≈ 15) the pressure loss should be calculated as $K_{tot} = \lambda l/d + \Sigma K_{loc}$ (Eq. (4)), because local losses are comparable to the friction loss. To separate them, the measurements should be repeated in a longer test section with the pressure taps at least 25d downstream of the inlet and with ΔP ≳ 25 Pa (U(ΔP) ≈ 7 %).

References

1. Pérez-Lombard, L., Ortiz, J., & Pout, C. (2008). A review on buildings energy consumption information. Energy and Buildings, 40(3), 394–398. https://doi.org/10.1016/j.enbuild.2007.03.007
2. International Energy Agency (IEA). (2018). The Future of Cooling: Opportunities for Energy-Efficient Air Conditioning. IEA, Paris. https://www.iea.org/reports/the-future-of-cooling
3. ShNQ 2.04.05-22. (2024). Isitish, ventilyatsiya va konditsiyalash [Heating, ventilation and air conditioning]. Urban planning norms and rules, approved by Order No. 01/2-39 of 5 August 2024 of the Ministry of Construction, Housing and Communal Services of the Republic of Uzbekistan (registered by the Ministry of Justice on 11 September 2024, No. 287; as amended). (in Uzbek). https://lex.uz/ru/docs/7262276
4. Darcy, H. (1857). Recherches expérimentales relatives au mouvement de l'eau dans les tuyaux. Mallet-Bachelier, Paris.
5. Moody, L. F. (1944). Friction factors for pipe flow. Transactions of the ASME, 66(8), 671–684.
6. Colebrook, C. F. (1939). Turbulent flow in pipes, with particular reference to the transition region between the smooth and rough pipe laws. Journal of the Institution of Civil Engineers, 11(4), 133–156. https://doi.org/10.1680/ijoti.1939.13150

7. ANSI/ASHRAE Standard 120-2017. (2017). Method of Testing to Determine Flow Resistance of HVAC Ducts and Fittings. American Society of Heating, Refrigerating and Air-Conditioning Engineers, Atlanta, GA.
8. COMSOL Multiphysics® (2023). CFD Module User's Guide. COMSOL AB, Stockholm, Sweden.
9. Launder, B. E., & Spalding, D. B. (1974). The numerical computation of turbulent flows. Computer Methods in Applied Mechanics and Engineering, 3(2), 269–289. https://doi.org/10.1016/0045-7825(74)90029-2
10. Menter, F. R. (1994). Two-equation eddy-viscosity turbulence models for engineering applications. AIAA Journal, 32(8), 1598–1605. https://doi.org/10.2514/3.12149
11. Spalart, P. R., & Allmaras, S. R. (1992). A one-equation turbulence model for aerodynamic flows. AIAA Paper 92-0439, 30th Aerospace Sciences Meeting and Exhibit, Reno, NV, USA.
12. Durbin, P. A. (1991). Near-wall turbulence closure modeling without "damping functions". Theoretical and Computational Fluid Dynamics, 3(1), 1–13. https://doi.org/10.1007/BF00271513
13. Wilcox, D. C. (2006). Turbulence Modeling for CFD (3rd ed.). DCW Industries, La Cañada, CA.
14. Shih, T.-H., Liou, W. W., Shabbir, A., Yang, Z., & Zhu, J. (1995). A new k-ε eddy viscosity model for high Reynolds number turbulent flows. Computers & Fluids, 24(3), 227–238. https://doi.org/10.1016/0045-7930(94)00032-T
15. Versteeg, H. K., & Malalasekera, W. (2007). An Introduction to Computational Fluid Dynamics: The Finite Volume Method (2nd ed.). Pearson Education, Harlow.
16. Ferziger, J. H., & Perić, M. (2002). Computational Methods for Fluid Dynamics (3rd ed.). Springer. https://doi.org/10.1007/978-3-642-56026-2
17. Celik, I. B., Ghia, U., Roache, P. J., Freitas, C. J., Coleman, H., & Raad, P. E. (2008). Procedure for estimation and reporting of uncertainty due to discretization in CFD applications. Journal of Fluids Engineering, 130(7), 078001. https://doi.org/10.1115/1.2960953
18. ASME V&V 20-2009 (R2016). Standard for Verification and Validation in Computational Fluid Dynamics and Heat Transfer. American Society of Mechanical Engineers, New York.
19. Çengel, Y. A., & Cimbala, J. M. (2014). Fluid Mechanics: Fundamentals and Applications (3rd ed.). McGraw-Hill Education, New York.
20. Altshul, A. D. (1982). Gidravlicheskie soprotivleniya [Hydraulic Resistance] (2nd ed.). Nedra, Moscow. (in Russian)
21. ASHRAE. (2021). Duct design. In ASHRAE Handbook—Fundamentals (SI ed., Chap. 21). American Society of Heating, Refrigerating and Air-Conditioning Engineers, Peachtree Corners, GA.
22. White, F. M. (2011). Fluid Mechanics (7th ed.). McGraw-Hill, New York.
23. JCGM 100:2008. Evaluation of measurement data — Guide to the expression of uncertainty in measurement. BIPM, Sèvres.